The formation of a hydroxyl bond and the effects thereof on bone-like apatite formation on a magnesia partially stabilized zirconia (MgO–PSZ) bioceramic following CO_2 laser irradiation

L. HAO*, J. LAWRENCE, K. S. CHIAN
Manufacturing Engineering Division, School of Mechanical and Production Engineering, Nanyang Technological University (NTU), 50 Nanyang Avenue, Singapore 639798
E-mail: haoliang@pmail.ntu.edu.sg

D. K. Y. LOW, G. C. LIM, H. Y. ZHENG
Singapore Institute of Manufacturing Technology, 71 Nanyang Drive, Singapore 638075

For the purpose of improving the bioactivity of a magnesia partially stabilized zirconia (MgO–PSZ) and to explore a new technique for inducing OH group and apatite formation, a CO_2 laser has been used to modified the surface properties. The bioactivity of the CO_2 laser modified MgO–PSZ has been investigated in stimulated human fluids (SBF) with ion concentrations almost equal to those in human blood plasma. Some hydroxyl groups were found on the MgO–PSZ following CO_2 laser treatment with selected power densities. The surface melting on the MgO–PSZ induced by CO_2 laser processing provides the Zr^{4+} ion and OH^- ion, in turn, the incorporation of the Zr^{4+} ion and the OH^- ion creates the Zr–OH group on the surface. After 14 days of SBF soaking, the apatites formed on the MgO–PSZ with relatively high amount of hydroxyl groups generated by the CO_2 laser treatment, while no apatite was observed on the untreated with few hydroxyl groups. It exhibits that the Zr–OH groups on the MgO–PSZ surface is the functional groups to facilitate the apatite formation. The increased surface roughness provides more active sites, meantime, increased surface energy benefits to the adsorption and reaction on the surface.

1. Introduction

For an artificial material to bond to living bone, it is essential that the material has the ability to form a biologically active, apatite layer on its surface in the human body. Under normal conditions, the body fluid is already supersaturated with respect to apatite, and once apatite nuclei form on the surface of a material, they can spontaneously grow by consuming the calcium and phosphate ions from the body fluid. The nucleation of apatite on the surface of a material is induced by the functional groups on its surface. When some components are released from the material into the body fluid and, thereby, increase the ionic activity product (IP) of the apatite, they can accelerate apatite formation [1].

The bioinert ceramics have attractive properties, such as high strength and fracture toughness for biomedical application. However, the integration between bioinert ceramic and tissue is a critical problem. There have been considerable efforts for improving the bioactivity of alumina and zirconia inert bioceramics. It has been revealed that a zirconia gel forms an apatite on its surface in a simulated body fluid (SBF), indicated that Zr–OH group is able to induce apatite nucleation [1]. Furthermore, the investigation of apatite-forming ability of zirconia gels with different structures exhibits that specific structures of Zr–OH group in tetragonal or monoclinic zirconia are effective for inducing apatite nucleation [2–4]. For the purpose of the apatite formation, the chemical treatment has been used to produce the Zr–OH group on a zirconia/alumina composite with high strength and fracture toughness subjecting the composite to H_3PO_4, H_2SO_4, HCl or NaOH aqueous solution treatments [5] and on zirconium metal treated with aqueous NaOH [6].

For the purpose of improving the bioactivity of the zirconia and explore a new technique for inducing OH group and apatite formation, a CO_2 laser has been used to modify the surface properties the magnesia partially stabilized zirconia (MgO–PSZ). To enhance the understanding the mechanism active in inducing bone-like apatite formation on the MgO–PSZ, the surface roughness, microstructure, crystal structure, chemical composition, surface energy and hydroxyl groups on the CO_2 laser modified MgO–PSZ were characterized.

*Author to whom all correspondence should be addressed.

The evaluation of bioactivity has been investigated in SBFs with ion concentrations almost equal to those in human blood plasma. The current study provides a novel technique and important information on introducing the bioactivity to the bioinert bioceramics.

2. Surface hydroxyl groups on zirconia

It is well known that, when exposed to the atmosphere, the surface of most oxidic systems becomes covered by a hydrated layer that builds up to compensate, at least in part, the coordinative insaturation of the surface ions brought about by the truncation of the crystallites. The surface hydrated layer is normally made up, in varying proportions, of hydroxyl groups belonging to the coordination sphere of one or more surface cations, and of undissociated water molecules coordinated to surface cations acting as Lewis acid centers. Relative amounts and stability toward thermal activation *in vacuo* of the two species in the surface hydrated layer depend primarily on the nature of the oxide system, and on the crystal planes constituting the termination of the crystallites [7]. In general, the second component of the hydrated layer (i.e. undissociated coordinated water molecules) may represent up to $\sim 50\%$ of the layer, is far less resistant to vacuum activation than surface OH groups (it is normally eliminated by $\sim 473\,K$), and is much less useful for the characterization of the surface features. In fact it is almost invariably associated with two unresolved $\nu(OH)$ bands at $\bar{\nu} \geq 3500\,cm^{-1}$, and with a broad $\delta(OH)$ band, centered at $\approx 1630\,cm^{-1}$ on all oxidic systems and on all crystal planes. Surface hydroxyls are, on the contrary, more useful for characterization work, as they are more sensitive to the coordinative and/or structural configuration of the surface cations to whose coordination sphere they are associated. Spectral data on the surface hydrated layer of m-ZrO_2 has reported that in general, an abundant component of undissocated water on m-ZrO_2; as well as two families of ''free'' surface hydroxyls absorbing at $\approx 3775\,cm^{-1}$ (termed $[OH]_H$) and $\approx 3675\,cm^{-1}$ (termed $[OH]_L$), respectively [7]. The two OH bands have usually been assigned to OH groups bonded respectively to one and more than one (possibly three) Zr^{4+} ions.

3. Bonelike apatite formation

Histological examinations *in vivo* show that an apatite layer is formed on the ceramic [8] surface early in the implantation period and, thereafter, the bone matrix integrates into the apatite. Detailed characterization indicates that this apatite layer consists of nano-crystals of carbonate-ion-containing apatite that has a defective structure and low crystallinity. These features are, in fact, very similar to those of the mineral phase in bone and, hence, bone producing cells, i.e. osteoblasts, can preferentially proliferate on the apatite, and differentiate to form an extracellular matrix composed of biological apatite and collagen. As a result, the surrounding bone comes into direct contact with the surface apatite layer. When this process occurs, a chemical bond is formed between the bone mineral and the surface apatite to decrease the interfacial energy between them. It can be concluded from these findings that an essential requirement for an artificial material to bond to living bone is the formation of a layer of biologically active bone-like apatite on its surface in the body.

It has been shown that the induction period for apatite formation decreases appreciably with an increase in pH or an increase in concentration of calcium or phosphate ions in the SBF [1]. This is attributed to an increase in the apatite IP of the SBF with an increase in the concentrations of the ions that constitute the apatite. The degree of the supersaturation of the apatite, increases with an increase in pH or an increase in the calcium- or phosphate-ion concentration of the SBF. The increased degree of the supersaturation increases the nucleation rate of the apatite, which results apparently in an increase in the quantity of deposited apatite. Once the apatite nuclei are formed, they grow spontaneously by consuming the calcium, phosphaste and hydroxyl ions from the surrounding fluid.

4. Experimental procedures

4.1. Material and CO_2 laser surface treatment

The material investigated was a 4% MgO–PSZ. The material was obtained in sheet form with dimension of $50 \times 50 \times 2.15\,mm^3$ (Goodfellow Ltd, USA). For experimental convenience, it was cut into blocks of $50 \times 12 \times 2.15\,mm^3$ with a diamond rimmed cutting blade. The material was used as received prior to laser treatment. A 3 kW CO_2 laser (Trumpf Ltd, Germany) emitting with a wavelength of 10.6 μm was used in this study. The laser produced a transverse electromagnetic mode (TEM_{01}) beam and was operated in the continuous wave mode. A series of optical units were used to deliver the CO_2 laser beam to the workpiece through the laser head, which was positioned by means of two linear (y- and z-axis) and rotary axes (b- and c-axis). The defocused CO_2 laser beam was traversed in single time across the surface of the MgO–PSZ samples placed on the stage using the x-axis. A series of experiments were conducted for a wide range of power densities with an 11 mm spot diameter, whilst the traverse speed was set at 2000 mm/min with 2 bars pressure O_2 process gas.

4.2. Characterization of the MgO–PSZ

The surface roughness (R_a) of the MgO–PSZ was measured by a profilometer (Surface Tester, SV-600). Five measurements were made at the different places on each sample and the mean values were obtained. The microstructure and crystal size of the MgO–PSZ were analyzed by scanning electron microscopy (SEM), optical microscopy and X-ray diffraction (XRD).

4.3. Surface energy analysis procedure

To investigate the effects of laser irradiation on the wetting and surface energy characteristics of the MgO–PSZ, a set of sessile drop control experiments were carried out using glycerol, formamide, etheneglycol, polyglycol E-200 and polyglycol 15–200 with known

total surface energy (γ_{lv}), depressive (γ_{lv}^{d}) and polar (γ_{lv}^{p}) component values [9]. The contact angles, θ, of the test liquids on the untreated and CO_2 laser treated MgO–PSZ were determined in normal atmospheric conditions at 25 °C using a sessile drop measure machine (First Ten Angstroms, Inc, USA). In order to estimate the influence of contaminant layers on the measurement results, the specimens of the untreated MgO–PSZ were cleaned with acetone in an ultrasonic bath for 2 h, rinsed with distilled water several times and dried in a vacuum oven at 90 °C for 12 h. The test liquids were used to measure θ for the cleaned sample. It was observed that the value of θ on the cleaned sample are 1.5, 1.2, 1.0, 0.9 and 0.8 for glycerol, formamide, etheneglycol, polyglycol E-200 and polyglycol 15–200, respectively, lower than that of the received sample without the cleaning. It is deemed that the contaminant on the surface of the MgO–PSZ has only a slight influence on the value of θ. Since the contaminant is a minor factor active in the wettability characterization, it is reasonable to preclude of cleaning pre-treatment for practical application of CO_2 laser treatment. In order to explore the potential of CO_2 laser treatment as an industrial and economical processing for altering the wettability of MgO–PSZ, the current research is conducted in an atmospheric environment without pre-cleaning. Each measurement of θ lasted for 3 min with profile photographs of the sessile drop being obtained every minute and a mean value being subsequently determined. After the test liquid drops for each liquid attached and rested on the MgO–PSZ surface, the drops consistently reached an equilibrium state in around 6 s. Thereafter they remained motionless and the magnitude of the θ changed little with time. On average only $\pm 0.5°$ deviation of the θ for each test liquid was observed during the 3 min of measuring when photographs were taken every minute; indicating that the shape of the drop was stable in its equilibrated state. The difference between the θ value on the left- and the right-hand side of the sessile drop is very small, which generates $\pm 0.36°$ deviations. In turn, the average total deviation for the θ measurement was $\pm 0.86°$.

4.4. FTIR Analysis

The optical adsorption spectra were measured at room temperature by means of a Fourier transform infrared spectrometer (FTIR) (Bio-Rad, US) spectrometer over the 500–5000 cm^{-1} range at a resolution of 1 cm^{-1}.

4.5. Soaking in SBF

The samples were soaked in an acellular human SBF [8], having an ion concentration nearly equal to that of human blood plasma. This solution, whose composition is reported in Table I, was prepared by dissolution of high purity reagents in distilled water, and was buffered at 7.25 with 50 mM Tris–hydroxymethyl amino ethane and 45 mM hydrochloric acid. The untreated and CO_2 laser treated samples with various power densities were immersed in 30 mL SBF in a polyethylene bottle at 37 °C, without stirring. After 14 days they were removed from the solution, gently washed in distilled water, and dried at room temperature. The soaked samples were then characterized by SEM and energy dispersive X-ray (EDX) analysis. The samples for SEM observations were simply dried and covered by a thin gold layer to guarantee the conductivity.

TABLE I Ionic concentration and pH of SBF in comparison with those in human blood plasma [8]

Ion	Concentration	
	Stimulated fluid	Blood plasma
Na^+	142.0	142.0
K^+	5.0	5.0
Mg^{2+}	1.5	1.5
Ca^{2+}	2.5	2.5
Cl^-	148.8	103.8
HCO_3^-	4.2	27.0
HPO_4^{2-}	1.0	1.0
SO_4^{2-}	0.5	0.5
pH	7.40	7.40

5. Results and discussion

5.1. Surface roughness and microstructure

Carbon-dioxide laser treatment brought about a consistently rougher surface on the MgO–PSZ compared with untreated sample, with the R_a increasing as the laser power density increased. The R_a was 0.295 μm (untreated), 0.305 μm (0.6 kW/cm^2), 0.333 μm (0.9 kW/cm^2), 0.717 μm (1.6 kW/cm^2), 1.882 μm (1.9 kW/cm^2), and 3.854 μm (2.5 kW/cm^2). The analysis revealed that the surface microstructure varied with the different CO_2 laser power density applied. The defined microstructures [10] according to the main structure on the MgO–PSZ were crystal reordering (0.6 kW/cm^2), hexagonal structure (0.9 kW/cm^2), cellular formation (1.6 kW/cm^2), uniform cellular structure (1.9 kW/cm^2), and coral and dendritic (2.5 kW/cm^2). The surface and cross-sectional images of cellular structure are shown in Fig. 1.

5.2. Phase transformation and crystal size effected by CO_2 laser irradiation

The diffraction patterns with 2θ between 28° and 32° of the untreated and CO_2 laser treated MgO–PSZ at various laser power densities are given in Fig. 2. A significant increase in the peak at 29° signifies that tetragonal phase is increasing. After CO_2 laser treatment, the peak at 29° shifts to 30.5° and was seen to rise, while the peaks at 28.2° and 31.5° disappear, indicating that the tetragonal phase is increasing while the monoclinic phase is decreasing. Moreover, the intensity of the peak at 30.5° assigned as (1 0 1) plane of the tetragonal lattice overwhelms the others, which indicates the tendency of crystal orientation. The crystal size in the direction perpendicular to the *hkl* plane, D_{hkl}, is expressed by the Scherrer equation [11],

$$D_{hkl} = \frac{K\lambda}{\beta \cos\theta} \quad (1)$$

where λ is the wavelength of the X-ray (1.54056 Å for K_α

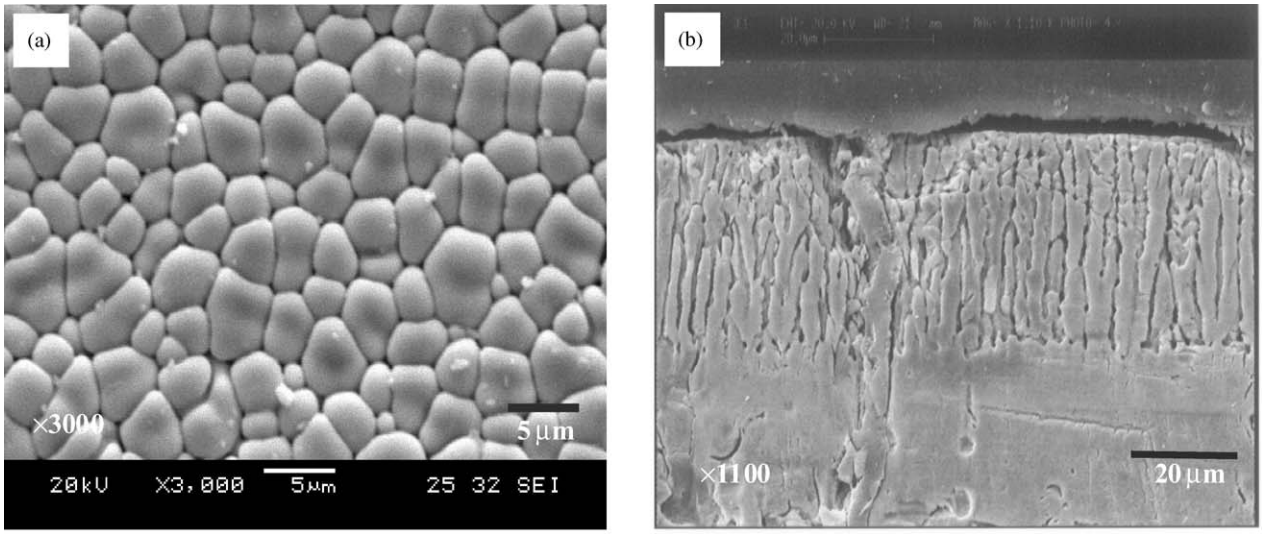

Figure 1 Typical optical view of a surface and SEM image of microstructure (a) on the surface and (b) cross-section view of CO_2 laser treated MgO–PSZ ($1.6\,kW/cm^2$).

line of Cu in this experiment), θ is the Bragg angle, β is the expansion of the XRD peak caused by the crystal size and K is the Scherrer constant. If one takes the FWHM of the peak at (101) as β, the crystallite size as D_{hkl}, and the K for 0.91, then the values of the crystal sizes on the MgO–PSZ obtained at various power densities obtained by XRD analysis were 34.7 nm (untreated), 41.6 nm ($0.6\,kW/cm^2$), 65.4 nm ($0.9\,kW/cm^2$), 103.1 nm ($1.6\,kW/cm^2$), 60.1 nm ($1.9\,kW/cm^2$) and 60.4 nm ($2.5\,kW/cm^2$).

5.3. Surface energy analysis

When a drop of liquid is brought into contact with a flat solid surface, the final shape taken by the drop is expressed by the contact angle, θ, which is related to the

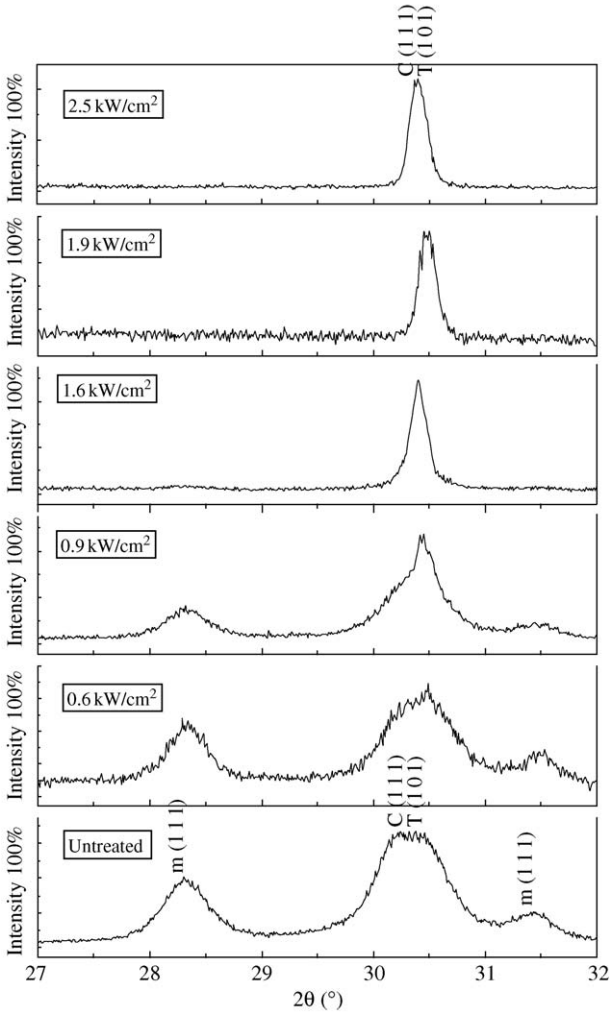

Figure 2 XRD analysis of the MgO–PSZ surface before and after CO_2 laser treatment with various power densities.

solid and liquid surface energies, γ_{sv} and γ_{lv}, and the solid–liquid interfacial energy γ_{sl}, through the principal of virtual work expressed by the rearranged Young's equation [12]:

$$\cos\theta = \frac{\gamma_{sv} - \gamma_{sl}}{\gamma_{lv}} \quad (2)$$

The majority of the forces are functions of the particular chemical nature of a certain material, and as such the total surface energy comprises γ^p (polar or non-dispersive interaction) and γ^d (dispersive component; since van der Waals forces are present in all systems regardless of their chemical nature). Thus, θ for solid–liquid systems where both dispersion forces and polar forces are present can be related to the surface energies of the respective liquid and solid by [13]

$$\cos\theta = \frac{2\left(\gamma_{sv}^d \gamma_{lv}^d\right)^{1/2} + 2\left(\gamma_{sv}^p \gamma_{lv}^p\right)^{1/2}}{\gamma_{lv}} - 1 \quad (3)$$

where γ_{lv}^p and γ_{lv}^d are the dispersive and polar component of liquid surface energy γ_{lv}, respectively. The determined results of surface energies of the untreated and CO_2 laser treated MgO–PSZ (at various power densities) are as shown in the Table II. It revealed that the CO_2 laser treatment increased the γ_{sv} surface energy of the MgO–PSZ through increasing γ_{sv}^p, since γ_{sv}^p was similar for all the samples and γ_{sv}^p was considerably different and thus generated the different γ_{sv}.

5.4. Spectral analysis and hydroxyl group

The main regions in the 750–950 cm^{-1} range are ascribed to ZrO_2 stretching modes as shown in Fig. 3, owing to the fact that it is similar to IR peak of the 20 mol % Al_2O_3 doped ZrO_2 nanoparticles reported previously [14] and the IR perk of the Al_2O_3–ZrO_2 nanopowders after laser ablation [15]. The vibration around 3300–3500 cm^{-1} in the FTIR spectra (see Fig. 4) could be attributed to the OH groups. Indeed OH stretching vibrations around this region have been observed by other workers on Al_2O_3–ZrO_2 nanopowders after Nd : YAG laser ablation [15] and on the Fe-doped crystals after laser irradiations [16]. As one can see from Fig. 4, the absorption coefficient of the OH group on the MgO–PSZ in this region increased after CO_2 laser irradiation and varied with the power density employed. For the untreated sample and the CO_2 laser treated sample (power density of the 0.6 kW/cm^2), the absorption peaks from 3200–3600 cm^{-1} are not obvious, indicating that no OH groups bonded on these samples. In contrast, the absorption peaks at this region can be

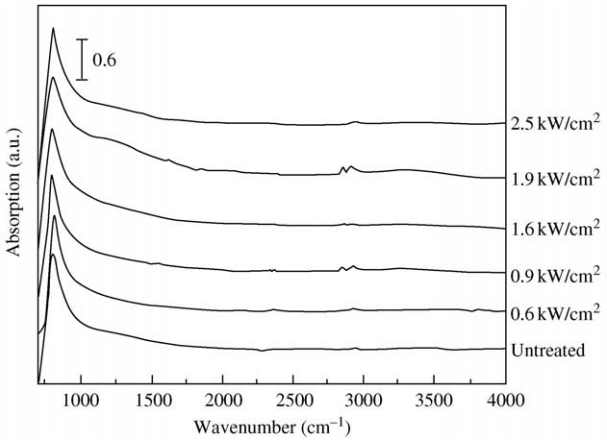

Figure 3 Infrared spectra of the untreated and CO_2 laser treated MgO–PSZ with different CO_2 laser power densities.

clearly observed on the samples following the CO_2 laser irradiation with power densities of 0.9, 1.6, and 1.9 kW/cm^2, denoting that OH groups existed on these samples. The highest absorption coefficient of OH groups was obtained on the sample that had been treated at 1.9 kW/cm^2. This finding shows that the OH groups increased with the CO_2 laser power density used. This relationship was also seen by Zeng *et al.* [17] on the OH groups bonded onto copper after CO_2 laser treatment. However, the absorption peaks in this region on the sample treated with a CO_2 laser power density of 2.5 kW/cm^2 was not obvious, suggesting that the OH bond does not increases linearly with the CO_2 laser power density. The explosive evaporation due to the superhigh temperature on the MgO–PSZ surface treated at this power density caused the water vaporization and disappearance of the OH-band. The phenomena of losing

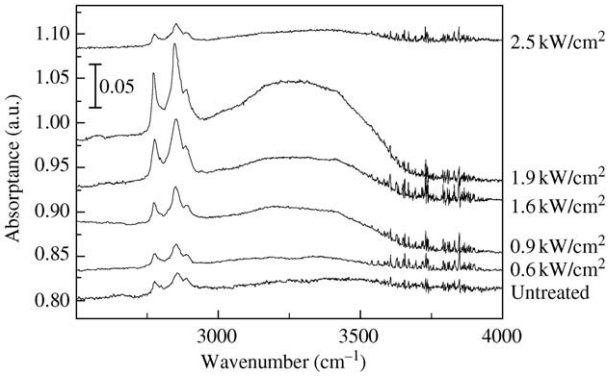

Figure 4 Infrared spectra of the hydroxyl groups present on the surface of the untreated and CO_2 laser treated MgO–PSZ with different power densities.

TABLE II Determined surface energy values for the MgO–PSZ before and after laser treatment of various power densities (traverse speed of 2000 mm/min)

Surface energy	Untreated	CO_2 laser treated (kW/cm^2)				
		0.5	0.9	1.6	1.9	2.5
Dispersive component γ_{sv}^d (mJ/m^2)	42.7	43.8	44.4	48.2	47.5	48.2
Polar component γ_{sv}^p (mJ/m^2)	10.1	10.4	21.9	60.7	33.2	26.7
Total surface energy γ_{sv} (mJ/m^2)	52.8	54.2	66.3	108.9	80.7	74.9

OH groups was also found on the human dentin after Er : YAG laser irradiation [18].

Carbon-dioxide, a weak acid, is known to absorb on ZrO_2 in the form of both carbonate and bicarbonate species [19]. Carbonate structures are formed via the interaction of CO_2 with zirconium cations in the lattice, as well as with a surface oxygen atom, whereas bicarbonate structures are formed via the interaction of CO_2 with hydroxyl group. The peak from 2800 to 3000 cm^{-1} testified to the existence of carbonate structures on the MgO–PSZ surface. The change of carbonate structures has the same trend as the OH groups discussed above.

The formation of the hydroxyl groups on the MgO–PSZ is due to the reactions of the zirconia with water vapour in air during CO_2 laser processing. Hydroxyl ion is a common impurity in insulating crystals; and by interacting with other impurities, it gives rise to new complexes. The OH-stretching frequency is a very sensitive probe of the hydroxyl environment. Proper thermal treatments and isotopic substitutions allowed to assign the stretching mode absorption lines to the defects in which OH^- is embedded and to supply possible models for them [19].

Crystal growth from the melt is commonly carried out in air atmosphere. Air always contains a certain degree of humidity from which OH^- ions are incorporated into the lattice [20]. CO_2 laser irradiation is a thermal process. When the laser fluence exceeds the ablation threshold, the irradiated surface experiences the melting, followed by evaporation, whereupon the particles emit from the surface. At a higher fluence, the amounts of particles increases and they break out quickly from the super-heated surface to produce a high density vapor plume wherein a portion of the particles are ionized due to the thermal ionization. Therefore, the main reactions occur in the melt ceramic and vapored flume:

$$ZrO_2 \Leftrightarrow Zr^{4+} + 2O^{2-} \tag{4}$$

So, the following oxido-reduction reactions occur at the melt-atmosphere interface:

$$O^{2-} \rightarrow \frac{1}{2}O_2 + 2e^- \tag{5}$$

$$H_2O + e^- \rightarrow \frac{1}{2}H_2 + OH^- \tag{6}$$

the whole reaction being

$$O^{2-} + 2H_2O \rightarrow 2OH^- + H_2 + \frac{1}{2}O_2 \tag{7}$$

Finally, the OH^- ions produced according to reaction (4) would be incorporated with one, two and three and four surface Zr^{4+}, respectively. According to the classification proposed by Tsyganenko *et al.* [21], the OH groups bonded in the spectral ranges at ~ 3770 and $\approx 3680\ cm^{-1}$ are typical one and three surface Zr^{4+} cations, respectively in tetragonal zirconia while the OH groups at ~ 3775 and $3675\ cm^{-1}$ bonds, respectively one and more than one (possible three) surface Zr^{4+} ion.

According to the microstructure analysis discussed, it has been found that the surface melting was occasioned on the MgO–PSZ treated by the CO_2 laser treatment with 1.6 kW/cm^2 power density [22]. Consequently, the Zr^{4+} ion and OH^- were produced and reaction between these ions brought about the Zr–OH group on the MgO–PSZ. The relatively high amounts of the hydroxyl groups bonded onto the modified samples with 1.6 and 1.9 kW/cm^2 were associated with the melting and chemical reaction on the MgO–PSZ surface.

5.5. The effects of CO_2 laser treatment on the MgO–PSZ in SBF and apatite formation

As one can see from Fig. 5, there are very small sediments on the untreated MgO–PSZ and CO_2 laser treated MgO–PSZ with the power density of 0.6 kW/cm^2. On the other hand, some obvious sediments are found on the CO_2 laser treated samples with the power densities of 0.9, 1.6, 1.9 and 2.5 kW/cm^2. The highest amount of the sediments is observed on the sample treated at 1.9 kW/cm^2. The EDX analysis shows that most particles on the soaked surface are NaCl sediments as the element of Na and Cl as shown in the Fig. 6(a).

Apatites were only found on the samples treated at power densities of the 1.6 and 1.9 kW/cm^2. As shown in Fig. 6(a), only a few apatites formed on the sample treated at a power density of 1.6 kW/cm^2 with only a small amount of Ca element shown in the EDX analysis given in Fig. 6(a). But, on the sample treated with a CO_2 laser power density of 1.9 kW/cm^2, some apatites were observed. One of them is shown in Fig. 6(b) with the Ca : P about 1.65. This Ca : P ratio exhibits the calcium phosphate transforms into apatite [8].

There was no occurence of apatite formation on the untreated and certain CO_2 laser treated samples (0.6, 0.9, 2.5 kW/cm^2) with few hydroxyl groups. On the other hand, some apatites formed on the CO_2 laser-treated samples (1.6 and 1.9 kW/cm^2) with some hydroxyl groups. This finding suggested that the hydroxyl group on the MgO–PSZ could be the predominant factor governing the formation of the apatites. The hydroxyl groups on the MgO–PSZ surface certainly generate Zr–OH groups which have been shown to be functional groups for the formation of the apatite [1], it is suggested that Zr–OH functional groups formed on the samples in the CO_2 laser processing at certain parameters and such functional groups naturally brought about the nucleation of the apatite on these samples in the SBF environment. The nucleation of the apatite could yield the apatite formation and bone-bonding ability to the MgO–PSZ modified to have Zr–OH groups on the surface.

The surface roughness and crystal size analysis showed that the CO_2 laser-treated samples at (1.9 and 2.5 kW/cm^2) has the rougher surface and larger crystal size than the untreated one. It is clear that the larger surface area could be favorable for producing more active sites on the surfaces and active hydroxyl sites. The similar result was found that the increased specific surface area on the heat-treated titanium was one of the factors active in inducing the apatite formation [23].

As shown in Table II, the CO_2 laser treated MgO–PSZ at relatively high power density have the higher surface energy than the untreated one and the samples treated at relatively lower power density. This was

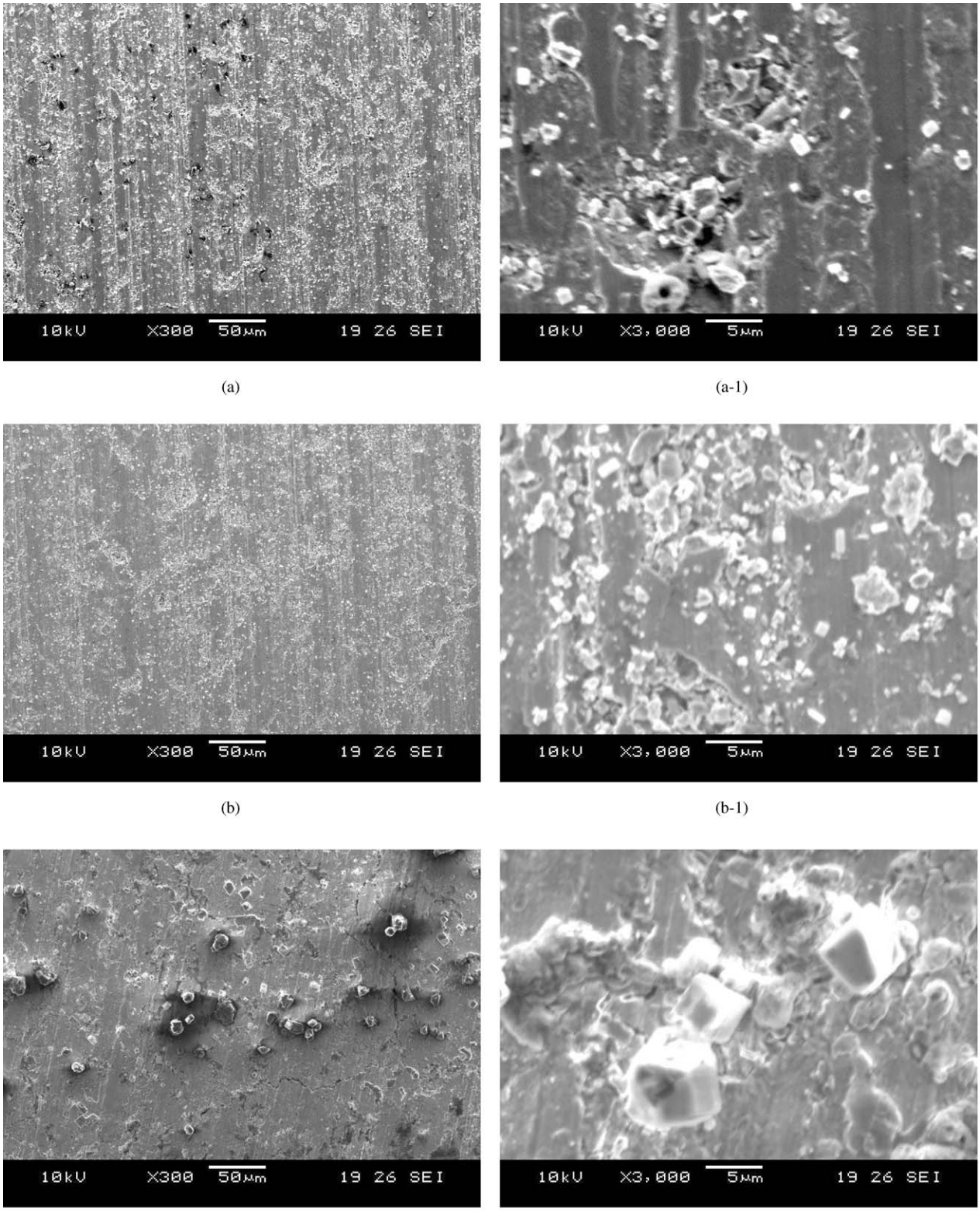

Figure 5 SEM images of the MgO–PSZ soaked in the SBF (a) Untreated (b) 0.6, (c) 0.9, (d) 1.6, (e) 1.9, (f) 2.5 kW/cm^2.

primarily attributed to the microstructure and phase change. It has found that there are more sediments and apatites on the surface with the higher surface energy than that on the surface with the lower surface energy. In the process of Ca–P precipitation, the variations of Gibbs function (ΔG) of the MgO–PSZ with the higher surface energy should be greater, compared to that of the MgO–PSZ surface with lower surface energy. This finding, agreeing with the study by Feng *et al*. [23], suggested that the adsorption and reaction would be more easily occurred on the surface with the higher surface energy, especially polar component of surface energy which would be beneficial to the chemical force and bonding.

6. Conclusions

The bioactivity of the CO_2 laser modified MgO–PSZ has been investigated in SBFs with ion concentrations almost equal to those in human blood plasma. The effects of

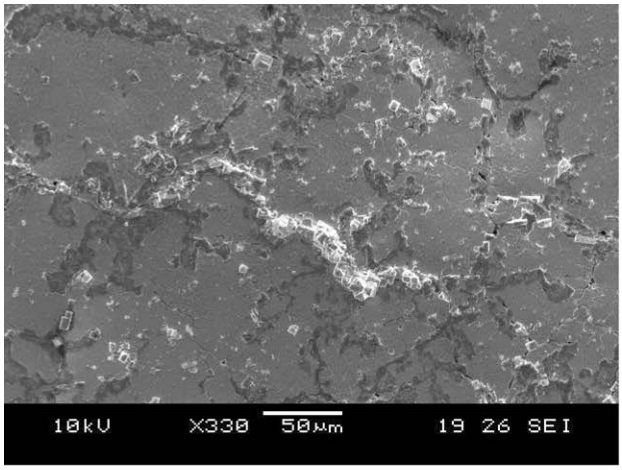

(d)

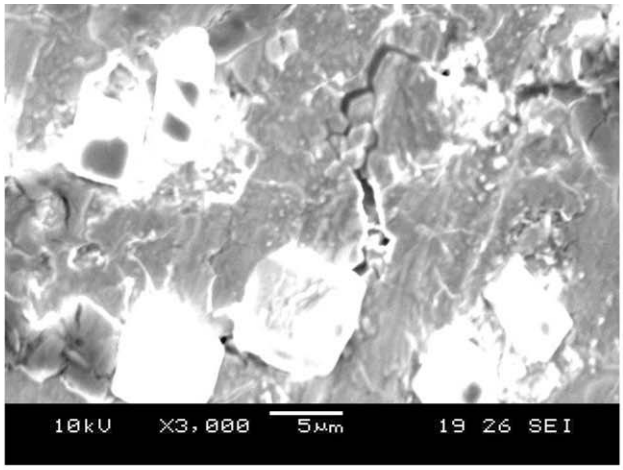

(d-1)

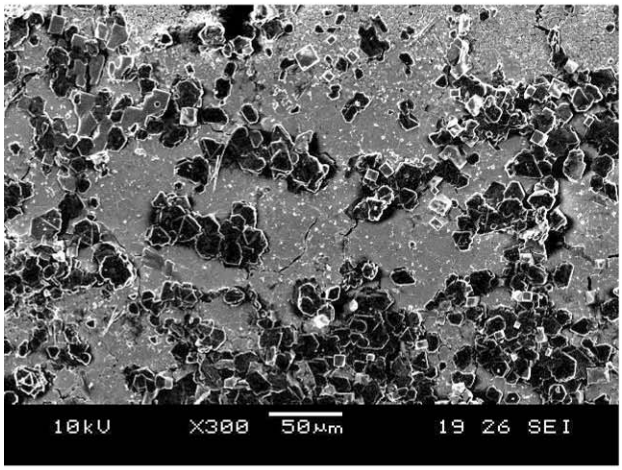

(e)

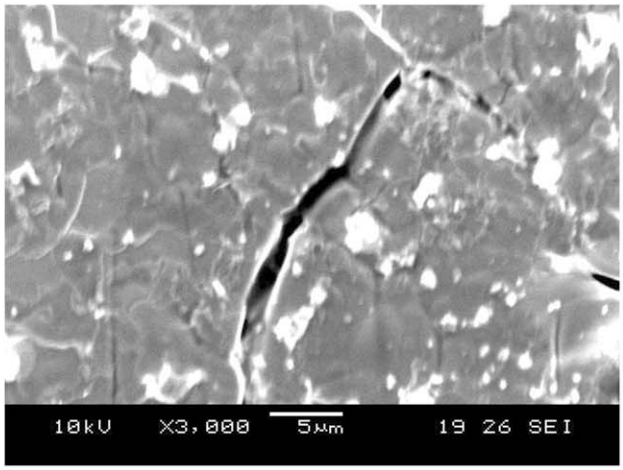

(e-1)

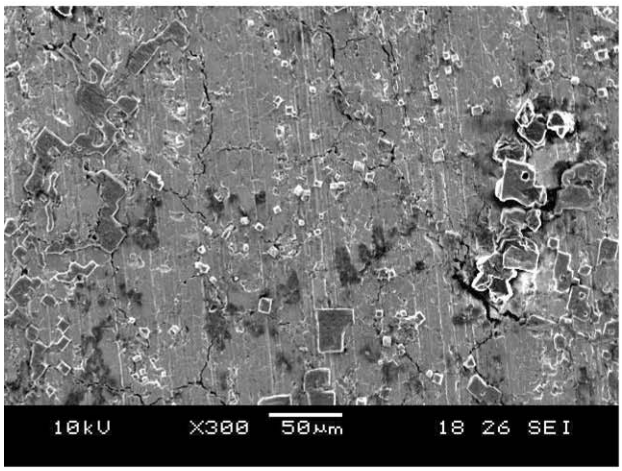

(f)

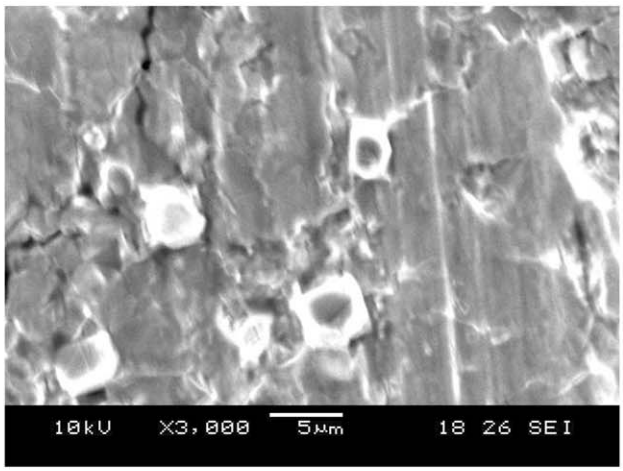

(f-1)

Figure 5 (Continued)

CO_2 laser irradiation on the hydroxyl groups and bone-like apatite formation has been analyzed. The conclusions can be drawn as follows:

1. It has been demonstrated that the CO_2 laser treatment could improve the bioactivity of the MgO–PSZ surface by generating functional group to facilitate the formation of bone-like apatites.

2. After 14 days SBF soaking, the apatite has formed on the MgO–PSZ with relatively high amount of hydroxyl groups generated by the CO_2 laser treatment with power density of 1.6 and 1.9 kW/cm^2, while no apatite has been observed on the untreated and CO_2 laser modified samples with few hydroxyl groups. It exhibits that the Zr–OH groups on the MgO–PSZ surface is the functional groups to facilitate the apatite formation.

3. The surface melting on the MgO–PSZ induced by CO_2 laser processing provides the Zr^{4+} ion and OH^- ion. The incorporation of Zr^{4+} ion and OH^- ion creates the Zr–OH group on the surface. However, the power

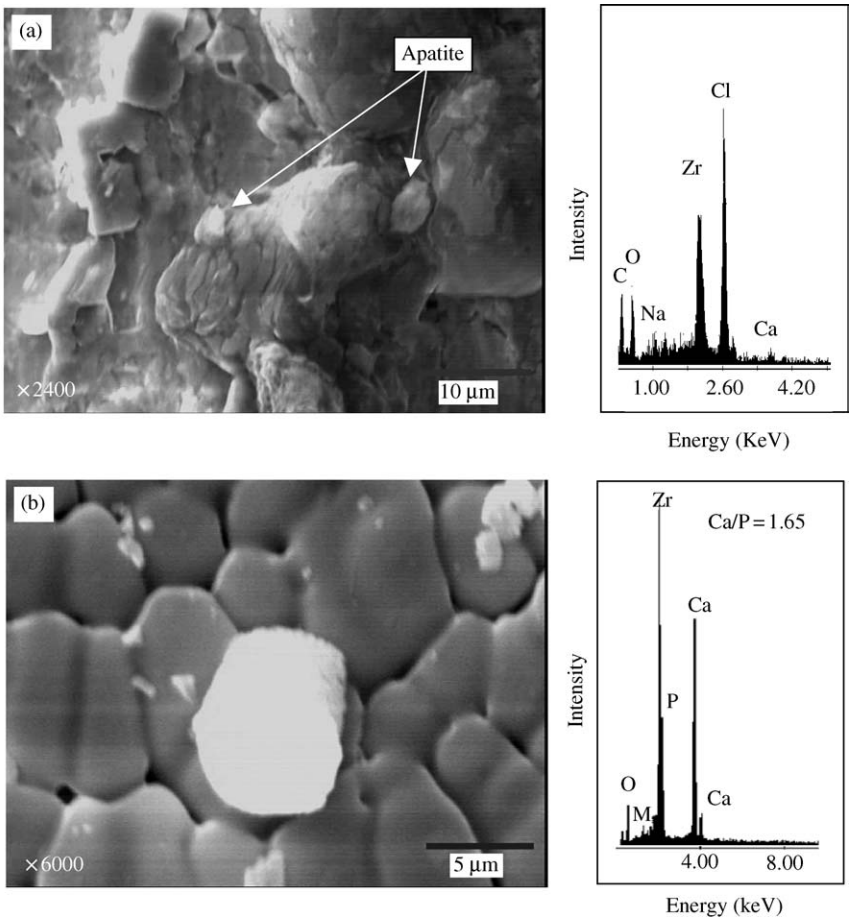

Figure 6 The SEM image and EDX analysis of the apatite formed on the MgO–PSZ treated at the power density of (a) 1.6 (b) 1.9 kW/cm^2.

density at 2.5 kW/cm^2 could generate the explosive evaporation and in turn lose the water and OH band.

References

1. M. UCHIDA, H. M. KIM, T. KOKUBO, F. MIYAJI and T. NAKAMURA, *J. Amer. Ceram. Soc.* **84** (2001) 2041.
2. M. UCHIDA, H. M. KIM, T. KOKUBO, K. TANAKA and T. NAKAMURA, *J. Ceram. Soc. Japan* **110** (2002) 710.
3. M. UCHIDA, H.-M. KIM, T. KOKUBO, M. NAWA, K. TANAKA and T. NAKAMURA, in 14th International Symposium on Ceramics in Medicine – Annual Meeting of the International Society for Ceramics in Medicine Bioceramics'01 (ISCM), November 2002, Palm Springs, CA, Trans Tech Publications Ltd. p. 637.
4. M. UCHIDA, H.-M. KIM, T. KOKUBO, S. FUJIBAYASHI and T. NAKAMURA, *J. Biomed. Mater. Res.* **64** (2003) 164.
5. M. UCHIDA, H.-M. KIM, T. KOKUBO, M. NAWA, T. ASANO, K. TANAKA and T. NAKAMURA, *ibid.* **60** (2002) 277.
6. M. UCHIDA, H. M. KIM, F. MIYAJI, T. KOKUBO and T. NAKAMURA, *Biomaterials* **23** (2002) 313.
7. C. MORTERRA, G. CERRATO, L. FERRONI and L. MONTANARO, *Mater. Chem. Phys.* **37** (1994) 243.
8. T. KOKUBO, H. M. KIM and M. KAWASHITA, *Biomaterials* **24** (2003) 2161.
9. A. J. KINLOCH, in ''Adhesion and Adhesives: Science and Technology'' (Chapman and Hall, London, 1987) p. 30.
10. L. HAO and J. LAWRENCE, *Proc. IMechE Part B, J. Eng. Manufac.* **218** (2004) 59.
11. P. SCHERRER, *Gottinger Nachrichten* **2** (1918) 98.
12. M. J. JAYCOCK and G. D. PARFITT, in ''Chemistry of Interfaces'' (John Wiley and Sons, Chichester, 1981) p. 234.
13. F. M. FOWKES, *Ind. Eng. Chem.* **56** (1964) 40.
14. Z. QIAN and J. L. SHI, *Nanostruct. Mater.* **10** (1998) 235.
15. X. C. YANG, W. RIEHEMANN, M. DUBIEL and H. HOFMEISTER, *Mater. Sci. Eng. B* **95** (2002) 299.
16. M. COCHEZ, M. FERRIOL, P. BOURSON and M. AILLERIE, *Optical Mater.* **21** (2002) 775.
17. D. W. ZENG, K. C. YUNG and C. S. XIE, *Appl. Surf. Sci.* **217** (2003) 170.
18. B. S. LEE, Y. L. HUNG and W. H. LAN, *Int. Congress Ser.* **1248** (2003) 143.
19. K. T. JUNG and A. T. BELL, *J. Mol. Catalysis A: Chemical* **163** (2000) 27.
20. L. MALICSKO and A. WATTERICH, *Nucl. Instr. Meth. Phys. Res. Sec. B: Beam Interact. Mater. Atoms* **191** (2002) 106.
21. A. A. TSYGANENKO and V. N. FILIMONOV, *Spectrosc. Lett.* **5** (1972) 477.
22. L. HAO and J. LAWRENCE *J. Phys. D: Appl. Phys.* **36** (2003) 1292.
23. B. FENG, J. Y. CHEN, S. K. QI, L. HE, J. Z. ZHAO and X. D. ZHANG, *J. Mater. Sci.: Mater. Med.* **13** (2002) 457.

Received 17 September 2003
and accepted 18 March 2004